2D Methods in NQR Spectroscopy *

R. Blinc and J. Seliger

J. Stefan Institute, University of Ljubljana, Ljubljana, Yugoslavia

Z. Naturforsch. **47a**, 333–341 (1992); received July 27, 1991

The application of two-dimensional spectroscopy to nuclear quadrupole resonance (NQR) is reviewed with special emphasys on spin 3/2 nuclei. A new two-dimensional level crossing double resonance NQR nutation technique based on magnetic field cycling is described. This technique allows for a determination of both the electric quadrupole coupling constant and the asymmetry parameter for spin 3/2 nuclei in powdered samples even in cases where the quadrupolar signals are too weak to be observed directly. It works if the usual double resonance conditions are met, i.e. if the spin-lattice relaxation times are not too short if the quadrupolar nuclei are dipolarly coupled to "strong" nuclei. Variations of this techique can be also used for 2D "exchange" NQR spectroscopy and NQR imaging.

Key words: 2D methods, NQR spectroscopy, Double resonance.

I. Introduction

Two-dimensional (2D) NMR and nuclear quadrupole resonance (NQR) spectroscopy [1], introduced by J. Jeener at the Ampere International Summer School in Baško polje, Yugoslavia (1971), exploits the possibility of manipulating the spin Hamiltonian so that it differs during the evolution (t_1) and data acquisition (t_2) periods (Figure 1). The free induction decay signal $S(t_1, t_2)$ thus depends on two variables, t_1 and t_2. The 2D spectrum is obtained by double Fourier transformation over t_1 and t_2:

$$S(\omega_1, \omega_2) = \int_{-\infty}^{+\infty} \int_{-\infty}^{+\infty} S(t_1, t_2)\, e^{i\omega_1 t_1}\, e^{i\omega_2 t_2}\, \mathrm{d}t_1\, \mathrm{d}t_2 . \quad (1)$$

While 2D spectroscopy has been widely used both in high resolution and solid state NMR, its application to NQR spectroscopy is just starting. Here we shall discuss those 2D NQR techniques which apply to spin 3/2 nuclei and enable one to obtain all three eigenvalues of the quadrupole coupling tensor from powder sample data.

We shall first review 2D Zeeman perturbed NQR spectroscopy [2] and 2D zero field NQR spectroscopy [3] both of which allow the determination of the asymmetry parameter η for polycrystalline powder samples in cases where it had previously only been obtainable from high field single crystal data. After that we shall describe a new level crossing double resonance 2D technique which allows for a determination of both the asymmetry parameter η and the electric quadrupole coupling constant e^2qQ/h in powder samples for $I = 3/2$ nuclei. In contrast to the above 2D NQR techniques it works also in cases, where the NQR signal is too weak to be directly observable. A modification of this technique, which allows for 2D NQR "exchange" spectroscopy experiments, is as well proposed.

II. 2D NQR Techniques

a) 2D Zeeman Perturbed Nuclear Quadrupole Resonance Spectroscopy [2]

For a system of quadrupolar nuclei of spin I in zero magnetic field, the pure NQR Hamiltonian is

$$\mathscr{H}_Q = \frac{e^2qQ}{4I(2I-1)} [3I_z^2 - \boldsymbol{I}^2 + \eta(I_x^2 + I_y^2)] . \quad (2)$$

The eigenvalues of $\mathscr{H}_Q$ are in the absence of a magnetic field degenerate with respect to $\pm m$. For $I = 3/2$ only

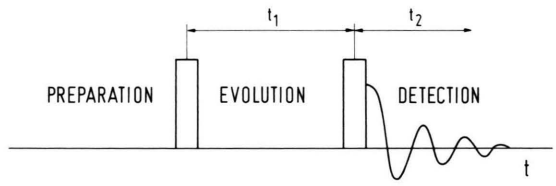

Fig. 1. Basic pulse sequence for 2D spectroscopy.

* Presented at the XIth International Symposium on Nuclear Quadrupole Resonance Spectroscopy, London, United Kingdom, July 15–19, 1991.

Reprint requests to Prof. R. Blinc, J. Stefan Institute, 61111 Ljubljana, Jamova 39, Yugoslavia.

0932-0784 / 92 / 0100-0333 $ 01.30/0. – Please order a reprint rather than making your own copy.

a single quadrupole resonance frequency is observed

$$\nu_Q = \frac{1}{2}\frac{e^2qQ}{h}[1+\eta^2/3]^{1/2}, \tag{3}$$

which is insufficient to determine the quadrupole coupling constant, e^2qQ/h, and the asymmetry parameter η separately. The application of a static magnetic field removes the degeneracy of the quadrupole energy levels. For polycrystalline samples where the static magnetic field $\boldsymbol{H}_0$ is applied parallel to the radiofrequency field $\boldsymbol{H}_1$, singularities occur in the powder lineshape [4] at

$$\nu = \nu_Q \pm \nu_L(1+\eta) \tag{4a}$$

and

$$\nu = \nu_Q \pm \nu_L(1-\eta)\,. \tag{4b}$$

Here $\nu_L = \gamma H_0$ is the Zeeman Larmor frequency. From the splitting of the singularities, which amounts to $2\nu_L\eta$ one can determine η. Standard Zeeman perturbed NQR is difficult in view of signal to noise problems and line overlaps associated with the presence of the static magnetic field. These problems are eliminated in the 2D Zeeman perturbed NQR scheme introduced in [2] as here the data acquisition takes place in zero external field.

The 2D pulse and magnetic field sequence [2] is shown in Figure 2a. In the preparation period a $\pi/2$ radiofrequency pulse is applied to the spin system and the static magnetic field H_0 is switched on. In the subsequent evolution period the spin magnetization is allowed to evolve for a time t_1 in the presence of both Zeeman and quadrupole interactions. During the detection period t_2 the static magnetic field is switched off and the magnetization evolves under the influence of the quadrupole interactions. By incrementing the t_1 values a two dimensional data matrix $S(t_1, t_2)$ is obtained which after a double Fourier transformation yields the 2D spectrum $S(\omega_1, \omega_2)$. The projection of the 2D spectrum on the ω_2 axis yields the zero field NQR spectrum, whereas the projection along the ω_1 axis gives the Zeeman NQR powder pattern multiplet structure. Cross sections parallel to the ω_1 axis yield the η values for the various nuclear sites.

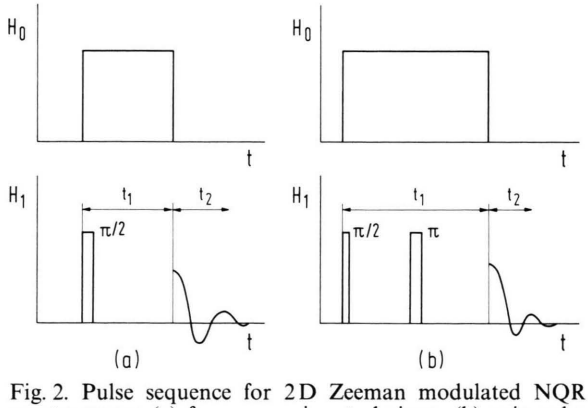

Fig. 2. Pulse sequence for 2D Zeeman modulated NQR spectroscopy: (a) free precession technique, (b) spin echo sequence technique.

A modification of the above procedure [2] is shown in Figure 2b, where a $\pi/2-\tau-\pi$ pulse sequence is used to produce an NQR spin echo. The $\pi/2-\tau-\pi$ pulse sequence is applied during the evolution period t_1 simultaneously with a static magnetic field H_0. The refocusing π pulse is applied in the middle of the evolution period. When the echo appears after $2\tau = t_1$, H_0 is turned off and the data are collected for a time t_2.

b) 2D Zero Field NQR Nutation Spectroscopy [3]

In the absence of an external frame of reference the pure NQR spectrum is orientation independent. In order to determine the principal values and orientation of the electric field gradient (EFG) tensor at the nuclear sites, an external static magnetic field can be applied producing orientation dependent spectra in single crystals and generating additional information in powder samples, as discussed in the previous section.

It is in fact not necessary to apply such an external static perturbation to obtain orientation dependent NQR spectra. The direction of the radiofrequency field $\boldsymbol{H}_1$ relative to the EFG (or quadrupolar) tensor axes introduces an orientation dependence in single crystal NQR spectra as well as singularities in the powder spectra [3], which allow for a determination of the asymmetry parameter.

The response of a quadrupolar nucleus with $\eta = 0$ to a radiofrequency (rf) pulse in zero external field has first been derived by Bloom et al. [5]. During an rf pulse a spin $I = 3/2$ nucleus undergoes nutation about the unique axis of its EFG (or quadrupolar) tensor. The strength of the effective H_1 field in a frame rotating about the quadrupolar axis depends on the relative orientation of the radiofrequency field H_1 and quadrupolar axis and goes to zero when these two axes are parallel. The nutation frequency is

$$\omega_N = (\sqrt{3}\,\omega_R \sin\theta)/2\,, \tag{5a}$$

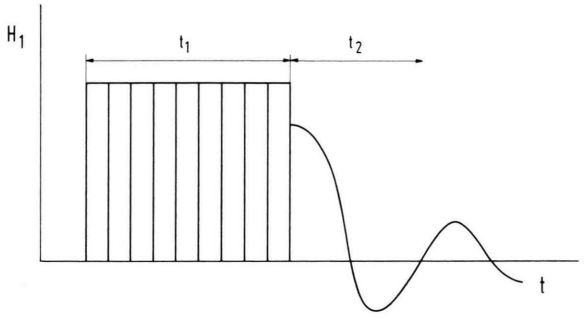

Fig. 3. Pulse sequence for 2D NQR nutation spectroscopy.

where

$$\omega_R = \gamma H_R = \gamma H_1 \tag{5b}$$

and θ is the angle between the coil and the largest quadrupolar principal axes.

The voltage induced in the coil by the precessing magnetization after the end of the rf pulse is also proportional to $\sin\theta$. The NQR free precession signal of a single crystal is thus in this case

$$S(t_1, t_2, \theta)_{\text{crystal}} = \text{const} \sin\theta \sin[\sqrt{3}\omega_R t_1 \sin\theta/2] \sin(\omega_Q t_2), \tag{6}$$

where t_1 measures the evolution time during which the rf field is turned on, t_2 measures the acquisition time during the free precession and ω_Q is the quadrupolar frequency. The 2D NQR spectrum is obtained by a double Fourier transformation over t_1 and t_2. The sequence is shown in Figure 3.

For a powder we have to perform in addition an integration over θ:

$$S(\omega_1, \omega_2)_{\text{powder}} = \text{const} \int_0^{\pi} \int_{-\infty}^{+\infty} \int_{-\infty}^{+\infty} \sin^2\theta \sin[(\sqrt{3}\omega_R t_1 \sin\theta/2] \cdot \sin(\omega_Q t_2)\, e^{i\omega_1 t_1}\, e^{i\omega_2 t_2}\, dt_1\, dt_2\, d\theta. \tag{6}$$

The corresponding 2D spectrum shows a single zero field NQR line at ω_Q in the ω_2 dimension and a powder pattern in the ω_1 dimension. The powder pattern exhibits [4] a singularity at the "perpendicular" edge, as in high field NMR.

The above technique can easily be extended to the case of an axially asymmetric EFG tensor [6]. Here the factor $\sin\theta$ has to be replaced by

$$R(\theta, \varphi) = \{4\eta^2 \cdot \cos^2\theta + [9 + \eta^2 + 6\eta\cos(2\varphi)]\sin^2\theta\}^{1/2}, \tag{7}$$

where θ and φ are the usual polar angles relating the quadrupolar frame to the coil axis. The time domain signal now becomes

$$S(t_1, t_2, \theta, \varphi) = \text{const}\, R(\theta, \varphi) \sin[\omega_R t_1 R(\theta, \varphi)/(2\sqrt{3}\varrho)] \sin(\omega_Q t_2), \tag{8}$$

where for $I = 3/2$

$$\omega_Q = e^2 q Q \varrho/(2h) \tag{9a}$$

with

$$\varrho = (1 + \eta^2/3)^{1/2}. \tag{9b}$$

Expression (8) of course reduces to (5) for $\eta = 0$.

The 2D spectrum of a powder sample is now obtained by double Fourier transformation over t_1 and t_2, as well as by a simultaneous integration from $0-2\pi$ and $0-\pi$ over φ and θ.

The powder spectra in the ω_1 domain show for $I = 3/2$ [4], as in high field NMR, three singularities at

$$2\pi\nu_1 = \frac{\eta\omega_R}{\sqrt{3}(1 + \frac{1}{3}\eta^2)^{1/2}}, \tag{10a}$$

$$2\pi\nu_2 = \frac{(3-\eta)\omega_R}{2\sqrt{3}(1 + \frac{1}{3}\eta^2)^{1/2}}, \tag{10b}$$

$$2\pi\nu_3 = \frac{(3+\eta)\omega_R}{2\sqrt{3}(1 + \frac{1}{3}\eta^2)^{1/2}}, \tag{10c}$$

which allow for a determination of η in a straightforward way.

III. 2D Level-Crossing Double Resonance NQR Nutation Spectroscopy

The two techniques discussed in the previous section can only be applied if the signal of the quadrupolar nucleus is directly observable. In many systems this is not the case in view of a too low NQR frequency or a to low natural abundance of the investigated nuclei. 2D spectroscopy can be applied in such a case as well with the help of double resonance techniques [7] which allow the observation of the "weak" quadrupolar nucleus via their effect on the signal of "strong" nuclei (e.g. the proton signal). These techniques work if the two kinds of nuclei are dipolarly coupled and the spin-lattice relaxation times (T_1) are long enough for double resonance manipulations to be performed.

Here we describe a new 2D NQR technique based on level crossing double resonance nutation spectroscopy. It allows for the simultaneous determination of

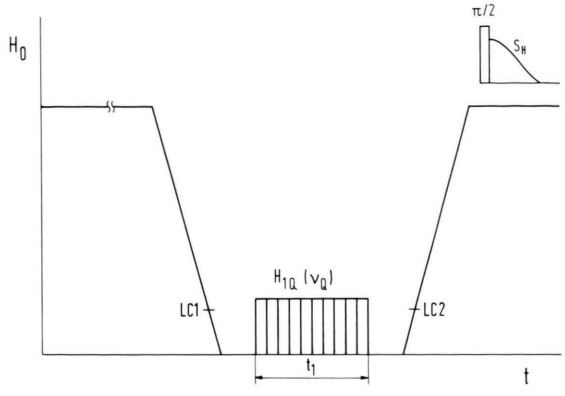

Fig. 4. Pulse sequence for 2D level crossing double resonance NQR nutation spectroscopy.

the zero field NQR spectra of quadrupolar nuclei, the signal of which is too weak to be directly observable, and the nutation spectra of these nuclei in the applied radiofrequency field which, among other things, allow for a determination of the asymmetry parameter η for $I=3/2$ nuclei in powdered samples. The level crossing is achieved by magnetic field cycling.

The scheme of the experiment is as follows (Figure 4): The nuclei with a strong NMR signal and a spin 1/2 (e.g. protons) are first polarized in a strong magnetic field H_0. After some time of the order or several T_1 the system is adiabatically demagnetized by decreasing H_0 to zero or moving the sample out of the magnet. At a certain field (LC1) level crossing [8, 9] takes place between the protonic Zeeman levels and Zeeman perturbed quadrupolar levels of the investigated quadrupolar nuclei. The level crossing polarizes the quadrupolar nuclei and decreases the proton magnetization. The polarized quadrupolar system is in zero static magnetic field irradiated with a strong radiofrequency field H_{1Q}, the frequency of which is

$$\omega = \omega_Q + \delta\,, \tag{11}$$

where ω_Q is the pure NQR transition frequency. The irradiation takes place for a time t_1. When $\delta=0$ and $\omega=\omega_Q$, the population $N_{\pm m}$ of the quadrupolar levels (say $\pm 1/2$ and $\pm 3/2$) is significantly changed by irradiation, thus decreasing the population difference $(N_{\pm 1/2}-N_{\pm 3/2})$. The proton system is remagnetized [8] after the second level crossing (LC2) with the quadrupolar system, and the resulting proton magnetization is measured by a resonant 90° radiofrequency pulse. The change in the proton signal is proportional to the population difference $(N_{\pm 1/2}-N_{\pm 3/2})$ and thus depends on t_1. The cycle is repeated for different irradiation times t_1 and different quadrupolar irradiation frequencies $\omega=\omega_Q+\delta$. When the quadrupolar irradiation frequency is resonant ($\delta=0$) the proton signal will show a dip. The Fourier transformation of the proton signal with respect to t_1 gives the ω_1 dimension, whereas the variation of the quadrupolar irradiation frequency $\omega=\omega_Q+\delta$ gives the ω_2 dimension in the 2D spectra. We thus deal with mixed frequency space-time space 2D experiment.

The evaluation of the NQR nutation spectra is performed with the help of the corresponding rotating frame density operator. The procedure is similar to the one used in the previous section. The difference is that here – because of the double resonance level crossing detection scheme – the population difference $(N_{\pm 1/2}-N_{\pm 3/2})$ and not the transverse component of the quadrupolar magnetization is observed.

If the direction of the radiofrequency field $\boldsymbol{H}_1$ with respect to the principal axes system of the electric field gradient tensor is characterized by the polar angle θ and the azimuthal angle φ (i.e. θ is the angle between $\boldsymbol{H}_1$ and the largest principal axis V_{ZZ}, whereas φ is the angle between the V_{XX} direction and the projection of $\boldsymbol{H}_1$ on the $V_{XX}-V_{YY}$-plane), we find (see Appendix) the part of the proton signal $S_H(t_1)$ which is proportional to the population difference $(N_{\pm 1/2}-N_{\pm 3/2})$ as

$$S_H(t_1) \propto (N_{\pm 1/2}-N_{\pm 3/2}) = A\cos[\omega(\theta,\varphi,\delta)\,t_1]\,. \tag{12}$$

Here A is a constant, $\omega(\theta,\varphi,\delta)$ is the nutation frequency of the quadrupolar nuclei

$$\omega(\theta,\varphi,\delta) = \sqrt{(\delta^2/4)+\omega^2(\theta,\varphi)} \tag{13a}$$

and

$$\omega(\theta,\varphi) = \frac{\omega_R}{2\sqrt{3+\eta^2}} \cdot \sqrt{4\eta^2+(9-3\eta^2)\sin^2\theta+6\eta\sin^2\theta\cos 2\varphi} \tag{13b}$$

with ω_R standing for

$$\omega_R = \gamma_Q H_1\,. \tag{13c}$$

γ_Q is the gyromagnetic ratio of the quadrupolar nuclei. The above expression for $S_H(t_1)$ is appropriate for a single crystal. In a powdered sample all orientations of the principal axes of the EFG tensors with respect to $\boldsymbol{H}_1$ are equally probable, and the expression (12) for $S_H(t_1)$ has to be replaced by

$$S_H(t_1) = \frac{S_H(0)}{4\pi}\int \cos[\omega(\theta,\varphi,\delta)\,t_1]\,d\Omega \tag{14}$$

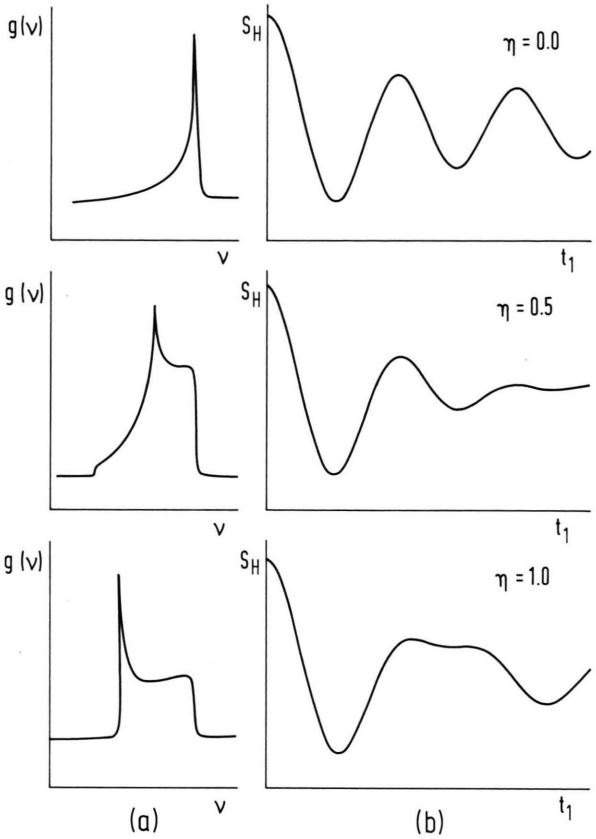

Fig. 5. (a) Calculated nutation powder lineshapes (in the ω_1 dimension) for a $I=3/2$ nucleus with the asymmetry parameter $\eta=0$, 0.5 and 1. (b) The corresponding double resonance signals $S_H(t_1)$ in the time domain t_1.

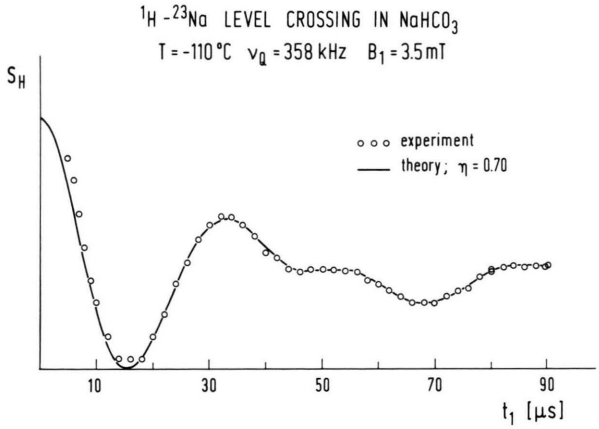

Fig. 6. Comparison between the experimental and theoretical ^{23}Na ($I=3/2$) double resonance nutation powder time domain (t_1) signal of $NaHCO_3$. The value of the asymmetry parameter is here $\eta=0.70$ and the value of ν_Q, obtained from the zero field NQR spectra in the ω_2 dimension, is 358 kHz.

The Fourier transform of $S_H(t_1)$ gives the frequency distribution function $g(\omega_1)$ which reflects the "powder" lineshape in the presence of the field $\boldsymbol{H}_1$. It has anomalies at the same position as expressions (10a)–(10c). The singularity occurs at the frequency given by (10b). The asymmetry parameer η can easily be determined from the difference between ν_3 and ν_2 divided by the sum of ν_3 and ν_2. The ω_2 dimension, on the other hand, reflects the zero field NQR spectra. The calculated nutation powder lineshapes $g(\omega_1)$ and the corresponding double resonance signals $S_H(t_1)$ are presented for some typical asymmetry parameters in Figure 5.

The experimental results obtained by the above technique in $NaHCO_3$ are presented in Figure 6. The specific advantage of the 2D level crossing double resonance NQR nutation spectroscopy technique is that e^2qQ/h and η can also be determined in cases like tris-sarcosine calcium chloride, where the ^{35}Cl NQR frequency is as low as 600 kHz and all other techniques fail because of a too low signal to noise ratio. The above technique has also been applied for the determination of order parameters in $Rb_{1-x}(NH_4)_xH_2PO_4$ type proton pseudo-spin glasses [10, 11] and other strongly disordered systems. It can also be modified to allow for the study of slow nucleus exchange processes by inserting between the evolution and detection periods an additional mixing period – where the quadrupolar Hamiltonian is changing due to exchange between different nuclear sites – in analogy to 2D exchange NMR techniques [12].

IV. 2D "Exchange" NQR and NQR Imaging

The 2D level crossing double resonance NQR technique described in the previous chapter can be easily modified (Fig. 7) with the addition of a "mixing" period to allow for the study of slow "exchange" processes via the observation of "cross-peaks". These cross peaks are – similarly as in NMR exchange spectroscopy [12] – due to the fact that the quadrupolar resonance frequency is changed in the "mixing" period due to nuclear exchange. The ω_1 dimension is as before given by the irradiation frequency whereas the ω_2 dimension is now obtained by incrementing the mixing period τ and performing the Fourier transformation with respect to τ.

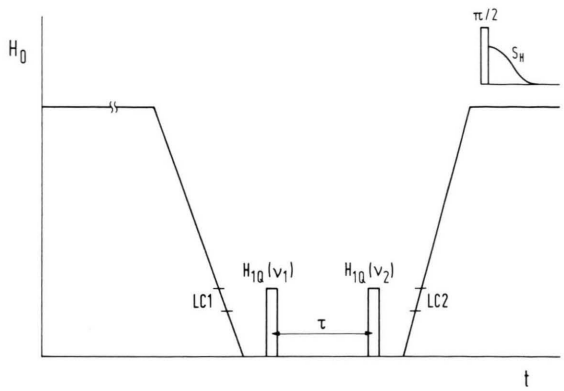

Fig. 7. Pulse sequence for 2D level crossing double resonance NQR "exchange" spectroscopy.

The experiment is performed as follows:

Let us assume that we have two chemically non-equivalent nuclear sites with different NQR frequencies $\nu_Q^{(1)}$ and $\nu_Q^{(2)}$ which are on the time average equally occupied: $P^{(1)}=P^{(2)}=1/2$. The spin-lattice relaxation times at the two sites have to be long enough to allow for a level crossing experiment to be performed.

The first level crossing (LC1) occurs at those values of the magnetic field where $\nu_H=\nu_Q^{(1)}$ and $\nu_H=\nu_Q^{(2)}$ (Figure 7). After the first level crossing the inverse spin temperature equals

$$\beta^{(1)}=\beta^{(2)}=\beta^{(0)}. \tag{17}$$

At zero field we now apply a strong radiofrequency pulse $\nu^{(1)}$ for a time τ_1 which saturates the NQR transition at $\nu_Q^{(1)}$. Immediately after this pulse we have

$$\beta^{(1)}=0, \quad \beta^{(2)}=\beta_0. \tag{18}$$

After a time t we get, because of nuclear exchange,

$$\beta^{(1)}=\frac{\beta^{(0)}}{2}(1-e^{-Wt}) \tag{19}$$

and

$$\beta^{(2)}=\frac{\beta^{(0)}}{2}(1+e^{-Wt}). \tag{20}$$

If we now apply at $t=\tau$ a second pulse at the frequency $\nu_Q^{(1)}$, we have immediately after the second pulse

$$\beta^{(1)}=0, \tag{21}$$

$$\beta^{(2)}=\frac{\beta_0}{2}(1+e^{-W\tau}). \tag{22}$$

The proton signal after the second level crossing (LC2) (Fig. 7) reflects the quadrupolar order:

$$S_H=S_{0,H}+K(\beta^{(1)}+\beta^{(2)}). \tag{23}$$

Here $S_{0,H}$ is the proton signal obtained for the case of a complete saturation of the two quadrupolar transitions ($\beta^{(1)}=\beta^{(2)}=0$ respectively $T^{(1)}=T^{(2)}=\infty$).

In the case when both pulses are applied at $\nu^{(1)}=\nu_Q^{(1)}$ we get

$$S_H=S_{0,H}+\frac{K\beta_0}{2}(1+e^{-W\tau}). \tag{24}$$

The same proton signal would be obtained if the two pulses would be applied at a frequency $\nu^{(2)}=\nu_Q^{(2)}$. Thus we get two diagonal peaks at $\nu_Q^{(1)}$ and $\nu_Q^{(2)}$.

If, however, we make a 2D experiment by varying both $\nu^{(1)}$ and $\nu^{(2)}$ we get for $\nu^{(1)}=\nu_Q^{(1)}$ and $\nu^{(2)}=\nu_Q^{(2)}$ (i.e. when the frequency of the first pulse is $\nu^{(1)}$ and of the second pulse $\nu^{(2)}$):

$$\beta^{(1)}=\frac{\beta_0}{2}(1-e^{-W\tau}), \quad \beta^{(2)}=0. \tag{25}$$

The corresponding proton signal after LC2 will now be

$$S=S_{0,H}+\frac{K\beta_0}{2}(1-e^{-W\tau}). \tag{26}$$

The probability of the nuclear exchange W can thus be determined by varying the exchange time τ in the mixing period and monitoring the resulting changes in the intensities of the diagonals

$$I_{diag}=\frac{K\beta_0}{2}(1+e^{-W\tau}); \quad \nu^{(1)}=\nu^{(2)}=\nu_Q^{(1)} \text{ or } \nu_Q^{(2)} \tag{27}$$

and off-diagonal peaks:

$$I_{cross}=\frac{K\beta_0}{2}(1-e^{-W\tau}); \quad \nu^{(1)}=\nu_Q^{(1)}; \quad \nu^{(2)}=\nu_Q^{(2)} \text{ or } \nu^{(1)}=\nu_Q^{(2)}; \quad \nu^{(1)}=\nu_Q^{(1)}. \tag{28}$$

The method works for W^{-1} lying in the interval 100 μs up to several second, i.e. when exchange is fast compared to T_1 cross-relaxation and spin diffusion effects.

The same modification can also be applied to 2D NQR nutation spectroscopy described in Section II b. Here the 2D "exchange" spectrum is obtained by incrementing the length of the mixing period τ and performing a 2D Fourier transform with respect to τ and aquisition time t_1.

Finally we should mention the possibility of *NQR imaging* via the use of strong radiofrequency field gradients. Special coils can be used to produce an inhomogeneous H_1 necessary to encode the spatial dimension in the NQR nutation experiment. Still another possibility is to use as the source of the required

H_1 inhomogeneity the the continuous attenuation of the radiofrequency field as it penetrates into a conducting sample [13]. This technique has been successfully used in a recent "skin-effect enhanced imaging" experiment. In a metal the H_1 field attenuates exponentially,

$$H_1 = H_{1,0} \exp(-x/\delta), \tag{15}$$

producing an rf field gradient

$$G = \left.\frac{dH_1}{dx}\right|_{x=0} = -H_{1,0}/\delta \tag{16}$$

at the surface. Here $\delta = 1/\sqrt{\pi \mu \sigma \nu_1}$ is the skin depth. For high H_1 fields, nutation frequencies of $\nu_1 = 150$ kHz for copper are obtainable, leading to $\delta = 10-30$ μm. This results in a field gradient of up to 20 T/cm at the surface, i.e. an extraordinarily large field gradient allowing for unprecented spatial resolution in solid samples [13, 14]. The described labelling of the spatial dimension by the nutation frequency allows for a simple one pulse nutation experiment. Incrementing the pulse length and performing a 2D transform with respect to pulse length and acquisition time leads to a 2D spectrum which shows the ordinary zero field NQR spectrum in the ω_2 and the spatial information in the ω_1 dimension. The technique may be particularly important for the study of surface. Double resonance detection as described in the previous section can be used here too.

Appendix

Evaluation of the Level-Crossing Double Resonance NQR Nutation Signal $S_H(t_1)$

Let us now derive expressions (12)–(14) and (23), which are basic for the understanding of 2D level-crossing double resonance NQR nutation spectroscopy.

Before the first level crossing (LC1) the two-level proton system is polarized in the magnetic field so that we have $(N_H/2)(1-\delta_0)$ protons on the upper and $(N_H/2)(1+\delta_0)$ protons on the lower energy level. For simplicity we assume that the quadrupolar system is unpolarized so that we have $N_Q/2$ quadrupolar nuclei on the upper and $N_Q/2$ nuclei on the lower level. After the first level crossing the quadrupolar system becomes polarized and the proton magnetization decreases as the inverse spin temperatures of the two systems become equal:

$$\delta'_H = \delta'_Q = \delta' = \delta_0(1-\varepsilon) \ldots . \tag{A.1}$$

Here

$$\varepsilon = N_Q/(N_Q + N_H) \tag{A.2}$$

stands for the ratio between the number of quadrupolar nuclei and the total number of nuclei $N = N_Q + N_H$.

Thus we have now $(N_H/2)(1-\delta')$ protons on the upper and $(N_H/2)(1+\delta')$ protons on the lower level. The corresponding populations for the quadrupolar system are $(N_Q/2)(1-\delta')$ and $(N_Q/2)(1+\delta')$. The polarized quadrupolar system is now in zero static magnetic field irradiated with a strong radiofrequency field H_{1Q} for a time t_1. This decreases the quadrupolar population difference if the frequency of H_{1Q} equals the pure NQR transition frequency. Before the second level crossing (LC2) the two systems spend a total time t in zero static field.

The inverse spin temperatures are in addition changed because of spin-lattice relaxation in zero field. Just before LC2 we thus have

$$\delta_H = \delta' \exp(-t/T_{1H}) \tag{A.3}$$

and

$$\delta_Q = \delta' \exp(-t/T_{1Q}) f(t_1), \tag{A.4}$$

where $f(t_1)$ describes the effect of the radiofrequency irradiation on the quadrupolar system. The proton system is remagnetized after the second level crossing (LC2) and we have

$$\delta''_H = \delta''_Q = \delta'', \tag{A.5}$$

where

$$\delta'' = \delta'(1-\varepsilon)\, e^{-t/T_{1H}} + \delta'\, \varepsilon\, e^{-t/T_{1Q}} f(t_1). \tag{A.6}$$

The proton signal which is measured after remagnetization with a 90° pulse, is proportional to δ''. We thus get

$$S_H(t_1) \propto \delta'' = A + B f(t_1). \tag{A.7}$$

If $t \leq T_{1Q}$ we can determine $f(t_1)$ by varying the irradiation time t_1 in zero magnetic field and measuring $S_H(t_1)$.

Let us now evaluate the form of $f(t_1)$. To do that we have to determine the effect of the radiofrequency irradiation on the form of the density matrix in the interaction representation. We shall carry out the calculation for an $I = 3/2$ quadrupolar nucleus.

In zero static magnetic field the Hamiltonian of the system is the sum of the quadrupolar Hamiltonian $\mathcal{H}_Q$ and the time dependent Zeeman Hamiltonian $\mathcal{H}_{rf}$ de-

scribing the interaction of the radiofrequency field H_{1Q} with the magnetic moment of the quadrupolar nucleus:

$$\mathcal{H} = \mathcal{H}_Q + \mathcal{H}_{rf} \tag{A.8a}$$

where

$$\mathcal{H}_{rf} = -\hbar\omega_R (\boldsymbol{I}\cdot\boldsymbol{n})\cos(\omega_Q t)\,. \tag{A.8b}$$

Here $\omega_R = \gamma H_{1Q}$, and the unit vector $\boldsymbol{n}$ describes the direction of the radiofrequency field $\boldsymbol{H}_{1Q}$ with respect to the X, Y, Z principal axes system of the EFG tensor. The frequency of the radiofrequency field is ω_Q. The angle between $\boldsymbol{n}$ and the direction of the largest principal axis V_{ZZ} is θ, whereas φ stands for the angle between the projection of $\boldsymbol{n}$ on the $X-Y$ plane and the direction of the V_{XX} principal axis.

Since the electric quadrupole coupling is invariant with respect to the reversal of the nuclear spin direction, no macroscopic magnetization is present in thermal equilibrium if $\mathcal{H}_{rf}=0$. The states $\pm m$ are thus degenerate. The presence of the radiofrequency field causes transitions between energy levels corresponding to different orientations of the electric quadrupole moment with respect to the electric field gradients, thus inducing an oscillating macroscopic nuclear magnetization.

In the presence of $\mathcal{H}_Q$ and $\mathcal{H}_{rf}$, the wave function for $I=3/2$ is expressed as a linear combination of eigenfunctions of $\mathcal{H}_Q$. We have now time dependent states:

$$|\pm a\rangle = c\,|\pm 3/2\rangle + s\,|\mp 1/2\rangle\,, \tag{A.9a}$$

$$|\pm b\rangle = -s\,|\pm 3/2\rangle + c\,|\mp 1/2\rangle\,. \tag{A.9b}$$

The calculation is performed in the interaction representation where the Hamiltonian is

$$\tilde{\mathcal{H}}_{rf} = \exp\{(i/\hbar)\,\mathcal{H}_Q t\}\,\mathcal{H}_{rf}\exp\{-(i/\hbar)\,\mathcal{H}_Q t\}\,. \tag{A.10}$$

It can be expressed in the $|a\rangle, |-a\rangle, |b\rangle, |-b\rangle$ representation as

$$\tilde{\mathcal{H}}_{rf} = -\frac{\hbar\omega_R}{2}\begin{bmatrix} 0 & \beta & -\alpha & 0 \\ \beta^* & 0 & 0 & \alpha \\ -\alpha & 0 & 0 & \beta \\ 0 & \alpha & \beta^* & 0 \end{bmatrix}. \tag{A.11}$$

Here

$$\alpha = S n_Z\,, \quad \beta = \frac{\sqrt{3}}{2} C n_- + \tfrac{1}{2} S n_+\,, \tag{A.12a}$$

$$S = 2c\,s\,, \quad C = c^2 - s^2\,, \tag{A.12b}$$

$$c^2 = \frac{1+\sqrt{1+\eta^2/3}}{2\sqrt{1+\eta^2/3}}\,, \quad s^2 = \frac{-1+\sqrt{1+\eta^2/3}}{2\sqrt{1+\eta^2/3}}\,, \tag{A.12c}$$

$$n_Z = \cos\theta\,, \quad n_+ = \sin\theta\, e^{i\varphi}\,, \quad n_- = \sin\theta\, e^{-i\varphi}\,. \tag{A.12c}$$

$\tilde{\mathcal{H}}_{rf}$ has two doubly degenerate eigenvalues

$$\lambda = \pm\sqrt{\alpha^2 + \beta\beta^*} \tag{A.13}$$

$$= \pm\sqrt{S^2 + \tfrac{3}{4}(C^2 - S^2)\sin^2\theta + \frac{\sqrt{3}}{2} CS\sin^2\theta\cos 2\varphi}$$

and the following eigen-states:

$$|\psi_1\rangle = \frac{1}{|\lambda|\sqrt{2}}(-\alpha, 0, |\lambda|, \beta^*); \qquad E_1 = -\frac{\hbar\omega_R}{2}|\lambda|, \tag{A.14a}$$

$$|\psi_2\rangle = \frac{1}{|\lambda|\sqrt{2}}(\beta, |\lambda|, 0, \alpha); \qquad E_2 = E_1\,, \tag{A.14b}$$

$$|\psi_3\rangle = \frac{1}{|\lambda|\sqrt{2}}(-\alpha, 0, -|\lambda|, \beta^*); \quad E_3 = \frac{\hbar\omega_R}{2}|\lambda|, \tag{A.14c}$$

$$|\psi_4\rangle = \frac{1}{|\lambda|\sqrt{2}}(\beta, -|\lambda|, 0, \alpha); \qquad E_4 = E_3\,. \tag{A.14d}$$

The density matrix in the interaction representation is now

$$\tilde{\sigma}(t) = \exp\{(i/\hbar)\,\mathcal{H}_{rf} t\}\,\sigma(0)\exp\{-(i/\hbar)\,\tilde{\mathcal{H}}_{rf} t\}$$
$$= T\sigma(0)\,T^*, \tag{A.15a}$$

where

$$\sigma(0) = \boldsymbol{I} - \delta'\begin{bmatrix} 1 & 0 & 0 & 0 \\ 0 & -1 & 0 & 0 \\ 0 & 0 & -1 & 0 \\ 0 & 0 & 0 & 1 \end{bmatrix} \tag{A.15b}$$

and $\boldsymbol{I}$ is the unity matrix. In the representation $|\psi_1\rangle$, $|\psi_2\rangle$, $|\psi_3\rangle$, $|\psi_4\rangle$, T is diagonal

$$T = \begin{bmatrix} e^{i\gamma t} & 0 & 0 & 0 \\ 0 & e^{i\gamma t} & 0 & 0 \\ 0 & 0 & e^{-i\gamma t} & 0 \\ 0 & 0 & 0 & e^{-i\gamma t} \end{bmatrix}, \tag{A.16a}$$

with $\gamma=\omega_1|\lambda|/2$. In the $|a\rangle$, $|-a\rangle$, $|b\rangle$, $|-b\rangle$ representation T is given by

$$T=\begin{bmatrix} \cos\gamma t & \frac{i}{|\lambda|}\sin\gamma t & -\frac{i\alpha}{|\lambda|} & 0 \\ \frac{i\beta^*}{|\lambda|}\sin\gamma t & \cos\gamma t & 0 & \frac{i\alpha}{|\lambda|}\sin\gamma t \\ -\frac{i\alpha}{|\lambda|}\sin\gamma t & 0 & \cos\gamma t & \frac{i\beta}{|\lambda|}\sin\gamma t \\ 0 & \frac{i\alpha}{|\lambda|}\sin\gamma t & \frac{i\beta^*}{|\lambda|}\sin\gamma t & \cos\gamma t \end{bmatrix} \tag{A.16b}$$

The level crossing experiment measures the diagonal elements of $\tilde{\sigma}(t)$. These are

$$\tilde{\sigma}(t)=\boldsymbol{I}-\delta'\begin{bmatrix} \cos 2\gamma t & 0 & 0 & 0 \\ 0 & -\cos 2\gamma t & 0 & 0 \\ 0 & 0 & -\cos 2\gamma t & 0 \\ 0 & 0 & 0 & \cos 2\gamma t \end{bmatrix}. \tag{A.17}$$

After a radiofrequencvy pulse of duration t_1 the population of the upper energy level is thus (for $T_{1Q}=\infty$) $(N_Q/2)[1-\delta'\cos(2\gamma t_1)]$ and the population of the lower energy level $(N_Q/2)[1+\delta'\cos(2\gamma t_1)]$. The function $f(t_1)$ is thus $\cos(2\gamma t_1)$. It can be explicitly expressed as

$$f(t_1)=\cos\left[\frac{\omega_R t_1}{2\sqrt{3+\eta^2}}\sqrt{4\eta^2+(9-3\eta^2)\sin^2\theta+6\eta\sin^2\theta\cdot\cos 2\varphi}\right]=\cos[\Omega t_1]. \tag{A.18}$$

We thus see that in a single crystal $f(t_1)$ depends on the orientation of $\boldsymbol{H}$ with respect to the principal axes of the EFG tensor at the investigated nuclear site. In a polycrystalline sample $f(t_1)$ is averaged over the solid angle:

$$f(t_1)=\frac{1}{4\pi}\int\cos[\Omega(\theta,\varphi)t_1]\sin\theta\,d\theta\,d\varphi. \tag{A.19}$$

The Fourier transform of $f(t_1)$ is the frequency distribution function $g(\omega_1)$, which exhibits singularities given by expressions (10a)–(10c).

[1] J. Jeener, Ampere International Summer School, Baško Polje, Yugoslavia 1971. See also R. R. Ernst et al., Principles of NMR in One and Two Dimensions, Oxford 1987.
[2] R. Ramachandran and E. Oldfield, J. Chem. Phys. **80,** 674 (1984).
[3] G. S. Harbison, A. Slokenbergs, and T. M. Barbara, J. Chem. Phys. **90,** 5292 (1989).
[4] Y. Morino and M. Toyama, J. Chem. Phys. **35,** 1289 (1961).
[5] M. Bloom, E. L. Hahn, and B. Hercog, Phys. Rev. **97,** 1699 (1955).
[6] J. C. Pratt, P. Rapanuthan, and C. A. McDowell, J. Mag. Res. **20,** 313 (1975).
[7] R. E. Slusher and E. L. Hahn, Phys. Rev. **166,** 332 (1960).
[8] R. Blinc, M. Mali, R. Osredkar, A. Prelesnik, J. Seliger, I. Zupančič, and L. Ehrenberg, J. Chem. Phys. **57,** 5087 (1972).
[9] D. T. Edmonds and P. A. Speight, J. Mag. Res. **6,** 265 (1972).
[10] R. Blinc, J. Dolinšek, R. Pirc, B. Tadić, B. Zalar, R. Kind, and O. Liechti, Phys. Rev. Lett. **63,** 2248 (1989).
[11] J. Dolinšek, J. Mag. Res. **92,** 312 (1991).
[12] C. Schmidt, B. Blümich, and H. W. Spiess, J. Mag. Res. **79,** 269 (1988).
[13] U. Skibbe and G. Neue, Colloids and Surfaces **45,** 235 (1990).
[14] G. Neue, Bruker Reports No. 2, 25 (1990).